Attitude Responses in Coupled Orbit-Attitude Dynamical Model in Earth–Moon Lyapunov Orbits

Amanda J. Knutson,* Davide Guzzetti,† and Kathleen C. Howell‡
Purdue University, West Lafayette, Indiana 47907-2045
and
Michèle Lavagna§
Politecnico di Milano, 20156 Milan, Italy

I. Introduction

THE circular restricted three-body problem (CR3BP) has been examined extensively in recent years; however, considerably fewer studies incorporate the effects of spacecraft attitude in this regime. Because of the sensitive nature of the dynamics at the libration points, a better understanding of the attitude motion of spacecraft in the vicinity of these points is warranted. The ability to predict the attitude motion of a spacecraft as orbital parameters and spacecraft characteristics are varied can be very useful. Similar studies are common in the restricted two-body problem. For example, the influence of spin rate, inertia characteristics, and orbit eccentricity on the attitude response are investigated by Kane et al. [1,2] in those works, and the consequences of the various parameters are effectively described using stability charts. Typically, stability charts display various configurations of a set of parameters and identify the reference motion as stable or unstable. Once the behavior is explored, the potential to exploit the natural dynamics for passive attitude control in these regimes is assessed.

In an early investigation, Kane and Marsh first consider the attitude stability of an axisymmetric satellite that is located exactly at the equilibrium points [3]. In their analysis, the satellite is artificially maintained at each of the equilibrium points and only the attitude motion is considered. Robinson continues this work with an examination of the attitude motion of both a dumbbell satellite [4] and an asymmetric rigid body [5] artificially maintained at the equilibrium points. Abad et al. introduce the use of Euler parameters in the study of a single rigid body located at L_4 [6]. More recently, Brucker and Gurfil explore the dynamics and stability of a single rigid-body spacecraft in the vicinity of the collinear points in the sun–Earth system, using Poincaré maps [7]. The effects of the gravity gradient torque are explored by these authors, but the spacecraft is still artificially fixed to the equilibrium point.

Wong et al. offer a detailed examination of the motion of a single rigid body near the vicinity of the sun–Earth libration points, using linear Lyapunov and halo orbit approximations [8]. The response of the spacecraft is detailed by Wong et al. in a meaningful manner, offering orientation results for a number of numerical simulations in terms of a body 3-2-1 (ϕ, θ, ψ) Euler angle rotation sequence. However, because the Lyapunov and halo orbits are represented in a linear form, the simulations are only valid for relatively small orbits close to the equilibrium points.

Recent investigations have examined the motion of a spacecraft located in various two- and three-dimensional periodic reference orbits, in the vicinity of the Earth–Moon collinear libration points. Lara et al. numerically investigate the attitude-orbit coupling of a large dumbbell satellite on halo and vertical L_2 orbits in the Hill problem [9]. If the spacecraft is in fast rotation and the equations of motion are averaged over the "fast" angle, the attitude dynamics of the dumbbell decouple from the orbital motion and the orbital dynamics simplify [10]. Studying this condition on halo and vertical L_2 orbits in the Hill problem, Lara et al. demonstrate that a sufficiently elongated structure may alter the stability of the reference periodic orbit [9]. Knutson and Howell explore the behavior of multibody spacecraft in the circular restricted three-body problem, using members of the nonlinear Lyapunov and halo orbit families as reference orbits, where the coupled orbit and attitude equations of motion are formulated using Kane's dynamic method [11–13]. Guzzetti et al. examine the coupled motion of a spacecraft in nonlinear Lyapunov reference orbits, in which the vehicle is only free to rotate in the orbital plane [14,15]. They formulate the equations of motion using a Lagrangian approach and also incorporate the effects of solar radiation pressure and flexible bodies. In both approaches, the equations of motion governing the orbit, as well as the spacecraft attitude, are blended in a cohesive manner that minimizes computational difficulties and allows for the propagation of meaningful results. One of the major and well-known computational issues in this process is the management of the disparity in length scales in this problem. The distance from the barycenter to the spacecraft is on the order of hundreds of thousands of kilometers (depending on the system), and the spacecraft dimensions are typically measured in terms of meters. The differences in the lengths present a computational challenge, because only finite precision is possible. Thus,

Received 24 December 2013; revision received 9 September 2014; accepted for publication 16 September 2014; published online 2 January 2015.

*Ph.D. Candidate, School of Aeronautics and Astronautics, Armstrong Hall of Engineering, 701 West Stadium Avenue; currently Princeton Satellite Systems, Inc., 6 Market Street, Suite 926, Plainsboro, NJ 08536.

†Ph.D. Student, School of Aeronautics and Astronautics, Armstrong Hall of Engineering, 701 West Stadium Avenue.

‡Hsu Lo Distinguished Professor, School of Aeronautics and Astronautics, Armstrong Hall of Engineering, 701 West Stadium Avenue. Fellow AIAA.

§Associate Professor, Department of Aerospace Engineering, Via La Masa 34.

a nonlinear variational form of the equations of motion is employed to mitigate these numerical effects. The motion of the spacecraft is also monitored relative to some known reference orbit. The equations for the time rate of change of linear momentum first describe the absolute motion of the spacecraft and are then again employed to describe the motion of the point mass reference system. The contributions from the reference are subtracted from the absolute motion, eliminating the difficulties of significantly different lengths coupled within the same differential equations.

The main goals in the current investigation include an examination of the effects of incorporating attitude dynamics into the model for the nonlinear periodic orbits within the context of the CR3BP, particularly the impact on vehicles in planar Lyapunov reference orbits. A more global understanding of attitude behavior in the CR3BP regime is also desired. To bring results from all planar family members together, the concept of an attitude map is employed, to visually display regions where the orientation is changing relative to the CR3BP frame. These maps are useful to summarize the results observed across a family and can offer insight into behavior that might not otherwise be observed.

II. Model

A. Problem Assumptions and Kinematic Framework

Consider a finite-sized rigid spacecraft with mass m whose behavior is influenced by the gravitational field of two other celestial bodies. No other forces but gravity are incorporated. The first and more massive body P_1 defines the primary attractor with mass m_1, denoted as the primary; similarly, the second attractor P_2 is called secondary with mass, such that $m_2 < m_1$. The dynamics of the spacecraft are modeled under the assumptions of the planar circular restricted three-body problem.

To the present, at least eight general approaches exist to deliver the equations of motion of a generic dynamic system [16,17]. Each formulation relies on different dynamic principles and choice of the free variables. In this work, to model the coupled problem, Kane's method is considered. However, before specifically developing the approach, it is necessary to supply a general framework for the kinematic representation of the problem. For the sake of clarity, each coordinate system is identified by a letter and the attendant versors by the same letter with a proper subscript; for instance, a generic X frame will be established by the $(\hat{\boldsymbol{x}}_1, \hat{\boldsymbol{x}}_2, \hat{\boldsymbol{x}}_3)$ term of versors. Let an inertial frame, denoted as the I frame, be fixed in the center of mass of the planetary system formed by P_1 and P_2. The $\hat{\boldsymbol{I}}_1$ versor of the I frame is initially aligned with the axis through the primary P_1 and the secondary P_2, but the I frame does not rotate with the planetary system. Define the ℓ frame to rotate with the bodies P_1 and P_2. The ℓ frame at time $t = 0$ is oriented parallel to the I frame and its origin corresponds to the origin of the I frame. Then, the ℓ frame rotates with the planetary system angular velocity Ω, such that the $\hat{\ell}_1$ versor is always aligned with the $P_1 - P_2$ line. The ℓ frame is intended as the common vector basis. With respect to this frame, the position of the spacecraft relative to the barycenter as origin is defined by the vector $\boldsymbol{R}$ with components $[xyz]^T$. Finally, a local coordinate system, the b frame, is fixed in the rigid body and attached to its center of mass B^*; a body 3-2-1 (ϕ, θ, ψ) Euler angle rotation sequence is assumed to describe the orientation of the b frame relative to the ℓ frame. Throughout this analysis, the main interest is on the first angle ϕ of the sequence, which is the angle of rotation between the body coordinate system and the ℓ frame about $\hat{\boldsymbol{I}}_3 = \hat{\ell}_3 = \hat{\boldsymbol{b}}_3$. The angle ϕ is labeled the pitch angle or simply pitch. If the vehicle only rotates about an axis orthogonal to the orbital plane, ϕ is sufficient to define the orientation of the body. Finally, the vectors $\boldsymbol{d}$ and $\boldsymbol{r}$ define the origin of the b frame relative to the primary and secondary, respectively. Figure 1 depicts all the coordinate systems.

For a finite-sized rigid spacecraft, the complete set of equations of motion is derived including both the orbit and attitude dynamics. Moreover, neither of the two motions is prescribed; instead, the fully coupled dynamics are simultaneously propagated. However, directly employing the vector $\boldsymbol{R}$ to track the satellite position is generally a poor choice for numerical solutions of the coupled equations of motion. The finite precision of the numerical procedure affects the problem in a twofold manner: First, computational difficulties arise because of the significantly different scales of the variables involved in orbital motion with respect to those appearing in the attitude dynamics; second, the actual mass extension of the body tends to vanish compared, again, to the distance from the barycenter of the celestial system. In fact, gravity does vary over the vehicle distribution of mass; this distribution yields minimal variations in the resultant gravity force, as well as in the well-known gravity gradient torque. To mitigate the numerical issues and to more accurately incorporate the small variations in the gravity force, the orbital motion is monitored relative to a given reference path. To this end, the equations describing the trajectory are rearranged into a nonlinear variational form via Encke's method. Basically, the dynamic contributions from the reference are subtracted from the absolute motion, eliminating different variable scales in the same set of differential equations. Hence, the orbital motion is integrated only in terms of the displacement from a reference path. More specifically, the reference trajectories are constructed as solutions of the CR3BP, which implies modeling the spacecraft as a mass with infinitesimal dimension. It should be noted that the reference orbits do not rely on any simplification of the CR3BP; conversely, they satisfy the nondimensional set of nonlinear equations

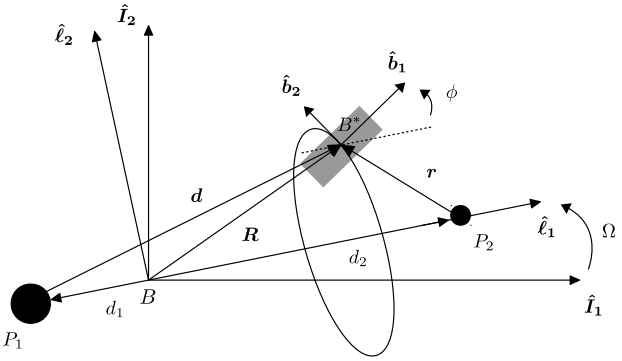

Fig. 1 Kinematic representation.

$$\ddot{x} - 2\dot{y} = x - \frac{(1-\mu)(x+\mu)}{d^3} - \frac{\mu(x-1+\mu)}{r^3} \tag{1}$$

$$\ddot{y} + 2\dot{x} = y - \frac{(1-\mu)y}{d^3} - \frac{\mu y}{r^3} \tag{2}$$

$$\ddot{z} = -\frac{(1-\mu)z}{d^3} - \frac{\mu z}{r^3} \tag{3}$$

where

$$d = \sqrt{(x+\mu)^2 + y^2 + z^2}, \qquad r = \sqrt{(x-1+\mu)^2 + y^2 + z^2}$$

The system is assumed to be normalized such that the following quantities appear unitary: the total mass of the system $m_1 + m_2$, the distance between the two attractor centers $d_1 + d_2$ (originally $d_1 + d_2 = 384,400$ km for the Earth–Moon system), the angular frequency Ω, and the universal constant of gravity G. The only parameter of the system that remains is the mass ratio $\mu = m_2/(m_1 + m_2)$ ($\mu = 0.01215$ for the Earth–Moon system).

B. Kane's Method

The formulation of Kane's equations is explored to model the problem. Kane's method is based on the principles of linear and angular momentum. However, the general formulas for the time rate of change of linear and angular momentum are partitioned into terms in the directions of a set of specified generalized speeds [18,19]. Generalized speeds, denoted u_i, are velocity variables that are

employed in the analysis in contrast to configuration coordinates (i.e., position variables); the generalized speeds can be selected in any manner, but it is usually desirable to adopt an independent set such that changes of one speed do not affect any other speed. If a set of minimal variables is selected, one generalized speed is required for each degree of freedom; otherwise, constraint equations are incorporated to reduce the order of the system. Eventually, the derivatives of the configuration coordinates, which may be required to fully describe the system, are formulated by some combination of a subset of the generalized speeds.

The b frame is selected as the common vector basis and an inertial observer is assumed for linear velocities, angular velocities, and time rates of change. Then, the following two equations are constructed:

$$\frac{\partial^I \boldsymbol{v}^{B^*}}{\partial \boldsymbol{u}} \sum \boldsymbol{F}^B - \frac{\partial^I \boldsymbol{v}^{B^*}}{\partial \boldsymbol{u}} \left\{ \frac{^I\mathrm{d}}{\mathrm{d}t} (m\, {}^I\boldsymbol{v}^{B^*}) \right\} = 0 \tag{4}$$

$$\frac{\partial^I \boldsymbol{\omega}^b}{\partial \boldsymbol{u}} \sum \boldsymbol{M}^{B/B^*} - \frac{\partial^I \boldsymbol{\omega}^b}{\partial \boldsymbol{u}} \left\{ \frac{^I\mathrm{d}}{\mathrm{d}t} ([I]^{B/B^*} \cdot {}^I\boldsymbol{\omega}^b) \right\} = 0 \tag{5}$$

where ${}^I\boldsymbol{v}^{B^*}$ represents the center of mass velocity and ${}^I\boldsymbol{\omega}^b$ the body angular velocity; $[I]^{B/B^*}$ is the spacecraft inertia matrix expressed in terms of the b frame, whereas $\boldsymbol{F}^B$ and $\boldsymbol{M}^{B/B^*}$ are, respectively, external forces and moments on the center of mass. The method employs simple matrix multiplications to derive the equations of motion. Thus, in Eq. (4), $\partial^I \boldsymbol{v}^{B^*}/\partial \boldsymbol{u}$ denotes the partial velocity matrix, which is formed from the partial derivatives of the center of mass velocity with respect to each generalized speed; the partial derivative of the velocity vector is evaluated for each generalized speed and this vector quantity is stored as a row in the partial velocity matrix. Similarly, in Eq. (5), $\partial^I \boldsymbol{\omega}^b/\partial \boldsymbol{u}$ is the partial angular velocity matrix for the body and it also originates from the partial derivatives of the angular velocity vector with respect to each generalized speed. Equations (4) and (5) are now summed to create one vector equation. Kane splits this equation into two parts: generalized inertia forces and generalized active forces. Generalized inertia forces, denoted $\boldsymbol{Q}_B^*$, combine the contribution of the quantities that depend on the time rate of change of both linear and angular momentum, and the generalized active forces, denoted $\boldsymbol{Q}_B$, collect the contributions from external loads. The generalized inertia force and generalized active force for the spacecraft are described as follows:

$$\boldsymbol{Q}_B^* = -\frac{\partial^I \boldsymbol{v}^{B^*}}{\partial \boldsymbol{u}} \left\{ \frac{^I\mathrm{d}}{\mathrm{d}t} (m_b^I \boldsymbol{v}^{B^*}) \right\} \quad - \frac{\partial^I \boldsymbol{\omega}^b}{\partial \boldsymbol{u}} \left\{ \frac{^I\mathrm{d}}{\mathrm{d}t} ([I]^{B/B^*} \cdot {}^I\boldsymbol{\omega}^b) \right\} \tag{6}$$

$$\boldsymbol{Q}_B = \frac{\partial^I \boldsymbol{v}^{B^*}}{\partial \boldsymbol{u}} \sum \boldsymbol{F}^B + \frac{\partial^I \boldsymbol{\omega}^b}{\partial \boldsymbol{u}} \sum \boldsymbol{M}^{B/B^*} \tag{7}$$

Finally, Kane's formulation is represented by the following simplified expression:

$$\boldsymbol{Q}_B^* + \boldsymbol{Q}_B = 0 \tag{8}$$

If more bodies are incorporated into the model, the generalized inertia forces and generalized active forces are computed for each body using the partial velocities matrices and the appropriate parts of the momentum equations as described in Eqs. (6) and (7). These two quantities are combined for each body, as described in Eq. (8); assuming workless constraints, the contact forces are automatically eliminated in Kane's method [18]. Thus, the governing equations are produced in the form $A\dot{\boldsymbol{u}} = \boldsymbol{w}$. This system of equations is integrated along with derivatives for the required configuration coordinates to determine the motion of the individual bodies in the system. The external forces and moments are only due to the gravity fields exerted by the two primaries on the vehicle; because the spacecraft is represented by a small rigid body, the expressions for both the gravitational forces and moments are approximated to the second-order expansion, as fully detailed in [19]. The resulting system is a coupled nonlinear set of equations. Additional details concerning this formulation and the development of a nonlinear variational form via Encke's method appear in [13].

C. Attitude Dynamics

Section II.B offers a viable method to derive the equations of motion for a rigid body of finite dimensions subjected to the gravitational attraction of two primary bodies. Subsequently, the analysis is focused on the planar rotational dynamics for a spacecraft moving along Lyapunov orbits about L_1 and L_2. Thus, for completeness, the rotational equations of motion are derived. First, define the location of the infinitesimal mass dm relative to the b frame

$$\boldsymbol{r}_{dm} = [\, x_{dm} \quad y_{dm} \quad z_{dm} \,]^T$$

and denote the body inertia matrix as $[I]^{B/B^*}$, where B^* denotes the body center of mass. Assuming the b frame is aligned to the body principal axes (relative to the center of mass), the inertia matrix reduces to a diagonal form

$$[I]^{B/B^*} = \begin{bmatrix} I_1 & 0 & 0 \\ 0 & I_2 & 0 \\ 0 & 0 & I_3 \end{bmatrix} \tag{9}$$

Adopting Kane's method, the rotational dynamics are derived from Eq. (5). The body angular velocities themselves (relative to an inertial frame) can be employed as generalized speeds; therefore, the partials matrix $\partial^I \boldsymbol{\omega}^b/\partial \boldsymbol{u}$ is equal to

$$\frac{\partial^I \boldsymbol{\omega}^b}{\partial \boldsymbol{u}} = \begin{bmatrix} 1 & 0 & 0 & 0 & 0 & 0 & 0 \\ 0 & 1 & 0 & 0 & 0 & 0 & 0 \\ 0 & 0 & 1 & 0 & 0 & 0 & 0 \end{bmatrix}^T$$

Additionally,

$${}^I\boldsymbol{\omega}^b = [\, \omega_1 \quad \omega_2 \quad \omega_3 \,]^T$$

The external moment vector of Eq. (5) only comprises the gravitational moment exerted by the two attractors, which, at the second-order approximation, is equal to (see [19])

$$\boldsymbol{M} = \frac{3\mu_1}{d^5} \int_m (\boldsymbol{r}_{dm} \times \boldsymbol{d}^b)\boldsymbol{d}^b \cdot \boldsymbol{r}_{dm}\, \mathrm{d}m + \frac{3\mu_2}{r^5} \int_m (\boldsymbol{r}_{dm} \times \boldsymbol{r}^b)\boldsymbol{r}^b \cdot \boldsymbol{r}_{dm}\, \mathrm{d}m \tag{10}$$

where μ_i is the planetary gravitational constant of P_i; the vectors $\boldsymbol{d}^b = [\, x_d^b \quad y_d^b \quad z_d^b \,]^T$ and $\boldsymbol{r}^b = [\, x_r^b \quad y_r^b \quad z_r^b \,]^T$ represent the position vectors of the spacecraft relative to the attracting bodies using the b frame as the vectorial basis. They can be related to the position coordinates $[\, x \quad y \quad z \,]^T$ relative to the planetary system center of mass by

$$\boldsymbol{d}^b = [A]^T \boldsymbol{d}, \qquad \boldsymbol{r}^b = [A]^T \boldsymbol{r} \tag{11}$$

where $\boldsymbol{d} = [(x+\mu)yz]^T$ and $\boldsymbol{r} = [(x+\mu-1)yz]^T$ and $[A]$ denotes the rotation matrix from the b frame to the ℓ frame. After some algebra,

$$\boldsymbol{M} = \frac{3\mu_1}{d^3} \begin{bmatrix} z_d^b y_d^b (I_3 - I_2) \\ x_d^b z_d^b (I_1 - I_3) \\ x_d^b y_d^b (I_2 - I_1) \end{bmatrix} + \frac{3\mu_2}{r^3} \begin{bmatrix} z_r^b y_r^b (I_3 - I_2) \\ x_r^b z_r^b (I_1 - I_3) \\ x_r^b y_r^b (I_2 - I_1) \end{bmatrix} \tag{12}$$

thus, the equations describing the rotational dynamics are

$$I_1 \dot{\omega}_1 = (I_3 - I_2) \left[\frac{3\mu_1}{d^5} z_d^b y_d^b + \frac{3\mu_2}{r^5} z_r^b y_r^b - \omega_3 \omega_2 \right] \tag{13}$$

$$I_2\dot{\omega}_2 = (I_1 - I_3)\left[\frac{3\mu_1}{d^5}x_d^b z_d^b + \frac{3\mu_2}{r^5}x_r^b z_r^b - \omega_1\omega_3\right] \tag{14}$$

$$I_3\dot{\omega}_3 = (I_2 - I_1)\left[\frac{3\mu_1}{d^5}x_d^b y_d^b + \frac{3\mu_2}{r^5}x_r^b y_r^b - \omega_2\omega_1\right] \tag{15}$$

With the further assumption of no rotations or displacements outside of the orbital plane of the attractors, $z_r^b = 0$, $\omega_1 = \omega_2 = 0$, and the rotation matrix $[A]$ is only function of the pitch angle

$$[A] = \begin{bmatrix} \cos\phi & -\sin\phi & 0 \\ \sin\phi & \cos\phi & 0 \\ 0 & 0 & 1 \end{bmatrix} \tag{16}$$

Consequently, the description of the attitude behavior reduces to a single first-order equation

$$\begin{aligned}\dot{\omega}_3 = {} & \frac{3\mu_1}{d^5}k_3[(y^2 - (x+\mu)^2)\sin\phi\cos\phi \\ & + (x+\mu)y(\cos^2\phi - \sin^2\phi)] \\ & + \frac{3\mu_2}{r^5}k_3[(y^2 - (x+\mu-1)^2)\sin\phi\cos\phi \\ & + (x+\mu-1)y(\cos^2\phi - \sin^2\phi)]\end{aligned} \tag{17}$$

where the inertia ratio

$$k_3 = \frac{I_2 - I_1}{I_3} \tag{18}$$

is introduced to represent the body shape.

III. Results

Alternative to the formulation from Sec. II, the Lagrangian formalism can be employed to develop the equations of motion, as presented in [14,15]. Using that formalism, an algorithm independent from Kane's method, can also be developed to reproduce the fully coupled dynamics of the spacecraft. Thus, two algorithms that differ in the choice of the kinematic variables, equations of motion, programming language, and programmer are actually implemented in this investigation. Of course, both methods address the same physical motion. All the results presented in this paper can be equally obtained by either formulation or algorithm. This capability also supports the validity of the outcomes, which are independently replicated in two different formulations.

A. Simulation Framework

This investigation is focused on understanding the attitude behavior across the Lyapunov families of periodic orbits about L_1 and L_2 in the Earth–Moon system. These families display a quasi-linear orbital response in the proximity of the equilibrium point; however, far from the equilibrium or libration point, the trajectories evolve under the effects of the fully nonlinear dynamics. In this scenario, the orbital dynamics along the family have been widely investigated, but little or no insight is available in terms of the natural attitude response. As discussed previously, some investigations have explored the problem, limiting the dynamic region of interest or considering specific point solutions. This work addresses a more global portrait of the phenomenon. Initially, the reference orbit is selected among the members of the L_1 or L_2 family, some of which are displayed in Fig. 2. The L_1 family spans an amplitude A_y (maximum displacement in the y direction over the single orbit) from 12,694 to 332,644 km, whereas the L_2 family extends from 11,889 to 181,648 km in the A_y direction. Alternatively, the L_1 family covers a range in orbital period from 11.77 to 31.72 days; the L_2 family of orbits ranges from 14.69 to 26.49 days.

In the next step, the spacecraft model is introduced. When the dynamics are planar, the displacements and the rotations of the vehicle only occur in the orbital plane of the attracting bodies. In such a case, assuming the b frame to be aligned with the body principal directions, only the inertia ratio k_3 defined in Eq. (18) (rather than the entire inertia tensor) is required to describe the rigid body distribution of mass, as modeled in Sec. II.C. By definition, the inertia ratio k_3 cannot be greater than one or smaller than -1. The inertia ratio k_3 controls the rotational dynamics regardless of the body shape, and the outcome is independent of the actual physical geometry of the spacecraft. However, to facilitate visualizing the physical implications of k_3, the spacecraft is assumed, without limiting the results, to be a rectangular plate lying in the orbital plane of the primaries. The plate possesses a uniform distribution of mass and the b frame is attached to the center of mass of the structure. The sides of the rectangle are aligned with the coordinates axes of the b frame. Thus, the b frame also represents the principal inertia axes. Given this configuration, $k_3 = 1$ represents a rod aligned along $\hat{\boldsymbol{b}}_1$ (the $\hat{\boldsymbol{b}}_2$ dimension disappears), $k_3 = -1$ represents a rod aligned along $\hat{\boldsymbol{b}}_2$ (the $\hat{\boldsymbol{b}}_1$ dimension disappears), and $k_3 = 0$ denotes a square plate. Varying the value of k_3 from zero to one, or -1, continuously stretches the initial square to a rectangle and eventually to a rod.

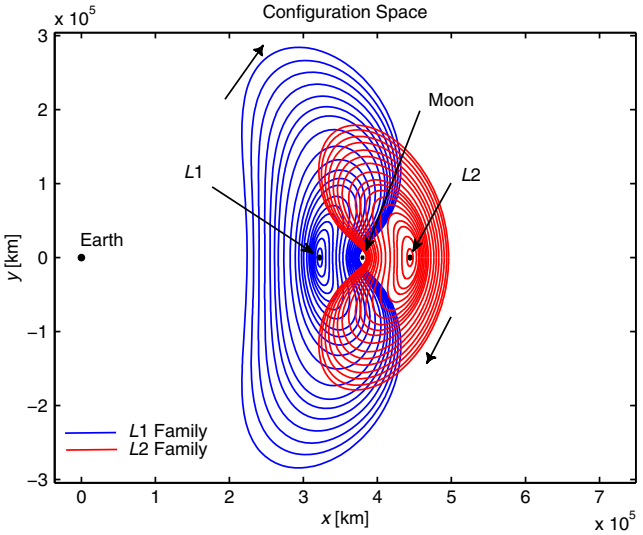

Fig. 2 Lyapunov families about the equilibrium point L_1 and L_2.

Finally, the spacecraft is located on the line through P_1 and P_2 ($\hat{\ell}_1$ axis) at the initial time. Specifically, the vehicle is placed on the left side of the equilibrium point, whereas the b frame is aligned with the ℓ frame. At $t = 0$, the body also appears to possess no initial angular velocity when observed in the ℓ frame. Maintaining these initial conditions, different simulations are completed by varying the reference orbit along the members of the family and by testing different spacecraft topologies via the variation of k_3 within the range $[-1, 1]$. In a set of infinite many combinations, this specific set of initial conditions is preferred because the principal axis of minimum inertia (for $k_3 > 0$) is initially aligned with the Earth–Moon line, which would represent a stable configuration if the spacecraft were to be artificially maintained along the same line. An increment of the initial pitch angle, currently $\phi(t = 0) = 0$ deg, would more likely trigger a diverging response. Similarly, moving the initial position of the spacecraft along the orbit would bring the vehicle closer to the Moon, which appears as a more sensitive dynamic environment. A large number of simulations are completed by varying the body shape k_3 and the reference Lyapunov orbit. Because each Lyapunov orbit is uniquely represented by its amplitude in the y or $\hat{\ell}_2$ direction A_y, the results are represented in terms of an A_y versus k_3 map. An attitude map essentially is a visual display of regions where the orientation remains aligned with respect to the ℓ frame (which represents the rotating frame in the CR3BP scenario) and, in contrast, regions where the orientation is changing relative to the ℓ frame. Specifically, in planar dynamics, the pitch angle ϕ is the only angle necessary to describe the spacecraft attitude. Thus, the attitude maps reflect the

time history for ϕ over one or more revolutions. On the map, the maximum pitch angle in the orientation history is reported by colors coding; a cutoff might be applied for a maximum value over an arbitrary threshold.

B. Mapping L_1 Lyapunov Orbits

The first map to be produced explores the planar Lyapunov family about L_1. Figure 3 represents the global response in ϕ, over one revolution, for each Lyapunov reference orbit. Darker colored areas correspond to conditions of motion where the body frame stays closely aligned with the rotating frame of the CR3BP, over one revolution. The darkest color corresponds to a rotation relative to the initial conditions of 0 deg ($\phi = 0$ deg for all the simulation time). However, a vehicle with fixed orientation relative to the ℓ frame is rotating about 13 deg /day in the Earth–Moon (E-M) system relative to an inertial observer, such as the I frame. For instance, over a Lyapunov orbit with a period of 11 days, a spacecraft that maintains a fixed orientation in the ℓ frame actually undergoes a rotation of 143 deg per revolution, as observed from the I frame. Therefore, dark areas predict a bounded response in the attitude as observed relative to the ℓ frame. Conversely, lighter areas are regions where the spacecraft orientation, in terms of pitch angle, is changing significantly relative to the CR3BP rotating frame. The lightest color on the map highlights angles greater than 90 deg relative to the initial orientation, over one revolution. From the map in Fig. 3, three clear regions of bounded responses over one orbit period appear; the expression "stable" is employed for a bounded response in the pitch angle ϕ as measured relative to the ℓ frame. Thus, a first stable zone is the vertical band centered around $k_3 = 0$. For $k_3 = 0$, the spacecraft is a perfect square and the gravitational torque (at the second-order approximation) is zero, supporting the "stability" of this region. A second region of bounded motions is the dark band near $A_y = 0$ km and $k_3 > 0$ (the bottom-right part of the plot); this region corresponds to the dynamic region investigated by Wong et al. [8], who examine quasi-linear orbits as a reference path. On a quasi-linear Lyapunov orbit, the oscillations of the pitch angle have limited amplitude as long as the minor inertia axis is initially aligned with the line through the primaries; in the given kinematic framework, that orientation corresponds to a positive k_3 value. Figure 4 shows a sample of quasi-linear Lyapunov orbits and the correspondent pitch angle solution. For the sake of completeness, a resonant condition in k_3 does exist in this motion regime [8]. Nonetheless, the amplitude of the oscillations grows quite slowly, such that the increment is not noticeable over one period in a map and this particular region appears as stable. As first observed by Knutson and Howell [11], a completely opposite behavior arises when nonlinearities in the orbital motion are incorporated (i.e., when the orbital amplitude increases). This behavior

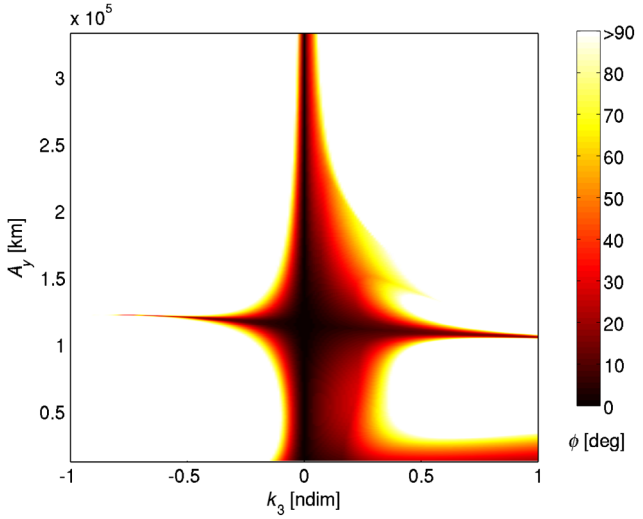

Fig. 3 Orientation response in ϕ for L_1 Lyapunov family (E-M system) over one revolution.

corresponds to the lightest area on the right side of the map, which denotes an attitude history diverging from the initial orientation. As discussed by Guzzetti et al. [14,15], the transition between the two regimes can be triggered as function of the orbit size as well as the body topology, but no specific characterization of the transition was previously provided. Moreover, it was postulated in [14,15] that it was not possible to naturally maintain the initial alignment of the body frame relative to the rotating frame over large Lyapunov orbits for elongated structures. The map confirms the existence of such a transition and also better characterizes the phenomena. A clear picture of the dynamics was not necessarily apparent when only considering specific test cases, as accomplished in the previous investigations.

New information also emerges from the map in Fig. 3. First, the shift from one regime to the other appears smooth. The smoothness of the transition suggests that small uncertainties in the investigated parameters do not lead to a drastic and sudden change in the attitude behavior. Second, quite unexpectedly, a third dark slightly diagonal band of small librations emerges from the map for a narrow set of Lyapunov orbits (near amplitudes $A_y \approx 1.1 \times 10^6$ km). Even in certain large reference orbits, spacecraft with specified inertia ratios, which lie on the dark line, remain relatively stable in orientation with respect to the CR3BP rotating frame. As visible on the map (light areas), the pitch response for elongated bodies ($|k_3| > 0.3$) along large Lyapunov orbits is generally unstable; however, the dark regions offer bounded solutions in a truly nonlinear orbital dynamics model for a fairly wide range of k_3 values. Moreover, negative as well as positive values of k_3 are included; this observation implies that the spacecraft could be stretched in both the coordinate directions relative to the b frame and small rotations might still exist. Beyond the horizontal dark band, the spacecraft always rotates more than 90 deg from the initial condition, if it possesses a geometry sufficiently extended in the $\hat{b}_2$ direction, which is the direction initially orthogonal to the line through $P_1 - P_2$. Different space structures, such as deep space gateway facilities or astronomical observatories [20], are proposed for flight in the vicinity of the Lagrangian points. The mass distribution of such architectures is unlikely axisymmetrical in the orbiting plan, yielding an inertia ratio k_3 certainly not zero. Such space structures or long-term facilities or habitats would be likely similar to those already flying near Earth, such as the International Space Station ($k_3 \approx 0.2$, [21]) or the Hubble space telescope ($k_3 \approx 0.6$).¶

Given the novelty of the horizontal stable zone about $A_y \approx 1.1 \times 10^6$ km in the attitude map, further steps are necessary to understand the coupling between the nonlinear orbital dynamics and the attitude response in these regions. The orbits involved in this phenomenon are depicted in Fig. 5: They span an amplitude range A_y from 101,108 to 114,621 km, one that corresponds to an interval from 17.57 to 19.04 days in terms of orbital period. It is worth noting that this span of orbital periods is located in the neighborhood of the two-thirds resonant ratio of the lunar period; a p/q resonant ratio implies that the spacecraft accomplishes q revolutions along the reference orbit (in the ℓ frame) in the same time interval that the Moon requires to complete p orbits about the Earth (in the I frame). In such a resonance, the Earth, the Moon, and the spacecraft return to the same inertial configuration after p lunar periods. Also, across this region an inversion of the direction of spin rotation occurs after the close approach to the Moon at 0.5 revolutions. Consider the example from Fig. 6 (which corresponds to $k_3 = 0.6$): A vehicle transiting along the smaller orbit in this amplitude region eventually spins counterclockwise (as observed in the rotating frame) after departing the $\hat{\ell}_1$ axis at the crossing closest to the Moon. Conversely, the ultimate direction of spin is clockwise, when the spacecraft is moving in the larger orbit in Fig. 6. Between these opposite behaviors, the pitch dynamics seem to transition smoothly from one limit to the other, generating the set of bounded responses that characterize this zone. Also, the nature of the stable response in this region is highly

¶Data available online at http://www.pha.jhu.edu/groups/hst10x [retrieved May 2014].

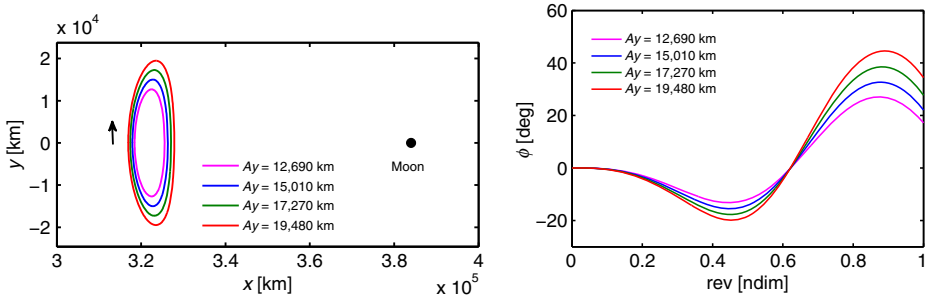

a) Set of L_1 planar lyapunov orbits (E-M system) **b) Pitch angle response**

Fig. 4 Orbital and attitude response in the quasi-linear region ($k_3 = 0.6$) over one revolution.

nonlinear and significantly differs from what it is observed in the quasi-linear zone (as seen in Fig. 4).

A further insight is offered from the eigenvalue analysis along the Lyapunov family. For each member of this family of periodic orbits, it is possible to compute the monodromy matrix and the associated eigenvalues. Given the symplecticity of the monodromy matrix, the eigenvalues occur in reciprocal pairs: One real pair is associated with the existence of planar manifolds, one unitary pair is associated with the periodic nature of the orbit and the existence of a family, and one pair corresponds to the out-of-plane dynamics. For planar Lyapunov orbits, the latter pair determines the changes of the eigenstructure throughout the family. Such mutations are usually investigated because they correspond to orbital bifurcations, but the attitude behavior may also relate to the eigenstructure. As apparent in Fig. 7, the orbits forming the stable horizontal band in the attitude map corresponds to the vicinity of the second of the Lyapunov family bifurcations. Specifically, the system mutates from hyperbolic to nonhyperbolic as the considered pair of eigenvalues shifts from the real axis to the unitary circle in the Argand–Gauss diagram. It is also noted that the quasi-linear stable region (terminating roughly at $A_y \approx 27,890$ km) encompasses one earlier bifurcation along the family (i.e., the first one at $A_y \approx 21,640$ km). Generally speaking, bifurcations indicate zones where the system is subject to a change of the dynamic regime; thus, it is reasonable that the transition in the orbital regime appears linked to the transition in the attitude regime. However, further investigations are necessary to completely understand this mechanism.

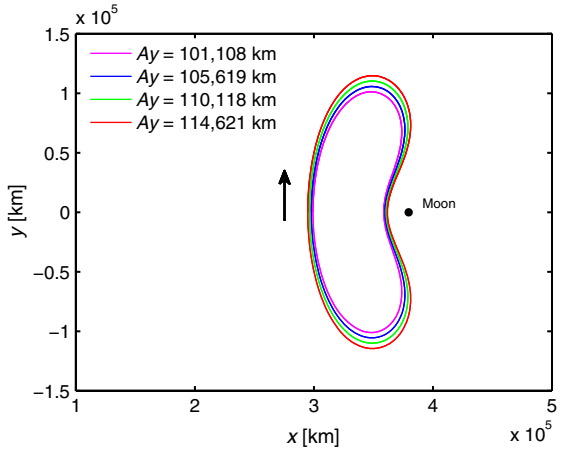

Fig. 5 Set of L_1 planar Lyapunov orbits (E-M system) in dark horizontal band region.

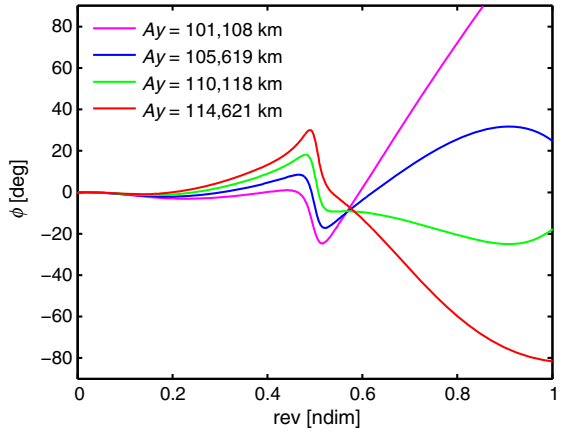

Fig. 6 Pitch angle response in dark horizontal band region ($k_3 = 0.6$) over one revolution.

C. Additional Maps

Under the coupled regime, any spacecraft naturally experiences a drift from the reference orbit as a consequence of its finite dimension. Therefore, the actual path nominally loses the periodicity property of the Lyapunov reference trajectory. No corrections are applied to restore the periodicity of the reference motion under the coupled dynamics in this analysis. As discussed previously [11,14,15], bodies with dimensions that are small compared with the distance from the attractors experience a significantly smaller drift from the orbit. Even if such deviation eventually leads to divergence because of the unstable nature of the nominal Lyapunov trajectories, within the time window observed here, the effects on the overall dynamic picture are negligible. Considering a space structure with a characteristic dimension of 100 m, Fig. 8 displays a comparison of the mapping obtained on the strictly nominal Lyapunov orbits and the mapping for the actual path, which include the drift from the reference. In Fig. 8, no visible differences are apparent. Thus, the lack of orbital periodicity over this time scale is not the significant factor influencing the attitude.

Thus far, the attitude map essentially offers a view of the natural attitude dynamics across the L_1 family after one revolution along each orbit. It is immediately evident that both the subject and the

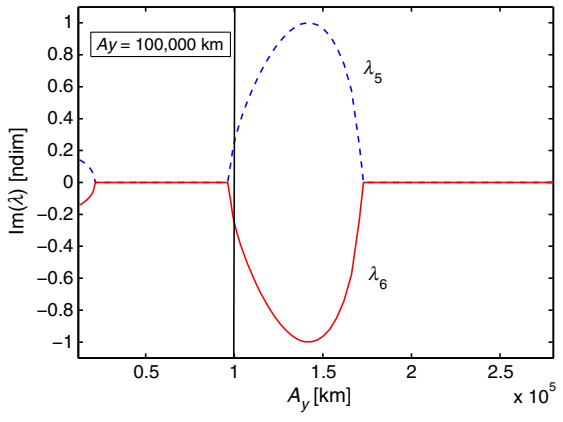

Fig. 7 Out-of-plane eigenvalues of the L_1 planar Lyapunov family.

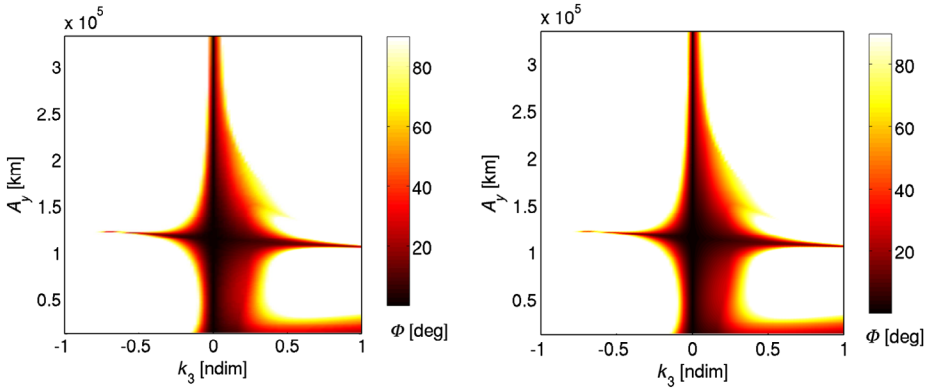

a) Nominal reference orbits **b) Actual path**

Fig. 8 Comparison of attitude mapping on reference and perturbed trajectories.

"exposure time" of such a portrait can be modified. First, the focus is maintained on the L_1 planar Lyapunov family, while increasing the observation time to two revolutions. No correction to the orbit or attitude is applied over the two revolutions. As a result, the attitude map in Fig. 9 emerges. Compared with the previous plot in Fig. 3, an overall reduction of the dark stable areas is perceived; specifically, the central horizontal band is disappearing and the bottom-right region is squeezed by an inflating unstable light zone. The vanishing of the horizontal band is more pronounced on the left side of the map, which corresponds to $k_3 < 0$, such that this region is now nearby completely (besides a minimal trace of the horizontal band) dominated by unbounded responses. Additionally, the transition to unbounded librations along the edge of the central vertical band becomes sharper. Given the current framework for the analysis, a structure mainly elongated in the $\hat{b}_2$ direction necessarily undergoes a natural rotation greater than 90 deg over a longer period. Conversely, spacecraft whose major extension is identified by $\hat{b}_1$ (i.e., $k_3 > 0$) still preserve some bounded solutions. However, it is noted that the bottom-right region, related to the pitch responses addressed by Wong et al. [8], significantly reduces in size and alters in outline. The linear behavior in Wong et al. [8] predicts an oscillatory response with limited amplitude, unless k_3 equals a critical value that triggers a resonance between the orbital frequency and the attitude librations. In a fully nonlinear regime, these predicted solutions hold true up to a certain amplitude of the quasi-linear orbits, as visible in Fig. 3. Increasing the integration time reduces the maximum orbit amplitude that guarantees a rotation less than 90 deg over the observation interval. In addition, the region in the vicinity of the linear resonant k_3 value (i.e., $k_3 \simeq 0.36$ in the Earth–Moon system) appears more unstable than observed over the time window of one revolution, as deducible from the light bulge that penetrates in the bottom-right dark area of Fig. 9, such that the latter zone almost splits into two regions.

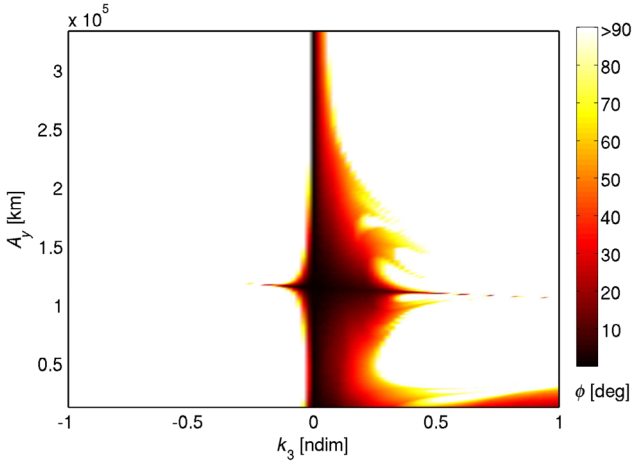

Fig. 9 Orientation response in ϕ for L_1 Lyapunov family (E-M system) over two revolutions.

Of course, not only the integration time but the orbital reference corresponding to the map can also be changed. Thus, the same procedure and the same structure of the initial conditions yields similar depictions for the L_2 family. In this case, the family spans an amplitude range in A_y from 11,889 to 181,648 km, which corresponds to a set of orbital periods from 14.69 to 26.49 days. The resulting attitude map appears in Fig. 10 for one revolution. Under the set of initial conditions investigated, there is no clear evidence of a central stable horizontal band in the L_2 family; a more predictable portrait comes to light. This map is characterized only by the central

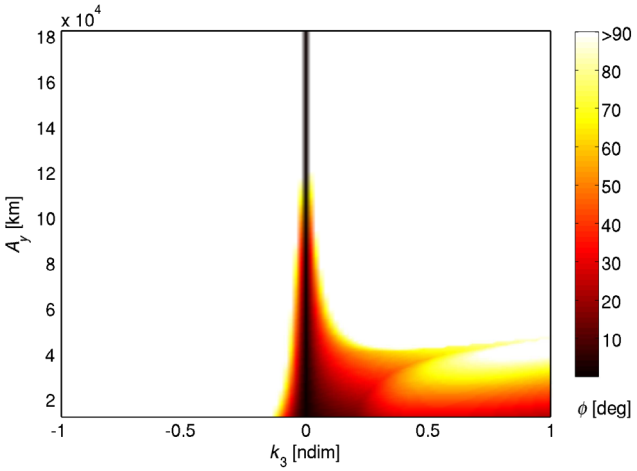

Fig. 10 Orientation response in ϕ for L_2 Lyapunov family (E-M system) over one revolution.

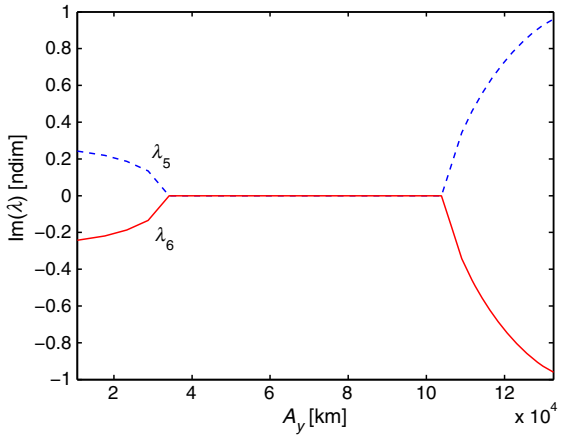

Fig. 11 Out-of-plane eigenvalues of the L_2 planar Lyapunov family.

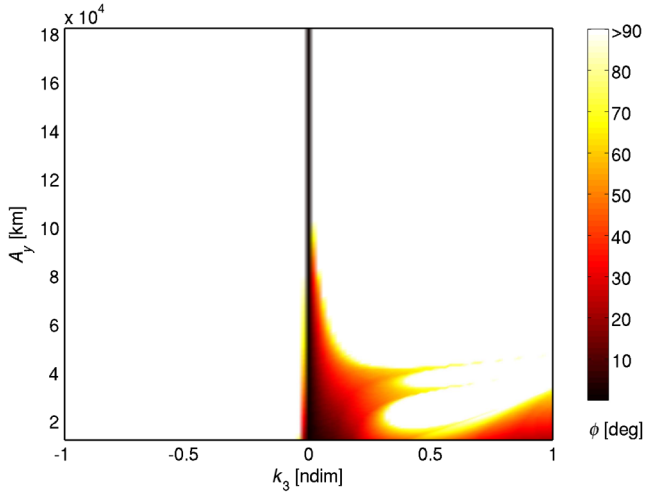

Fig. 12 Orientation response in ϕ for L_2 Lyapunov family (E-M system) over two revolutions.

vertical band associated with a value $k_3 = 0$ and the bottom-right region, corresponding to the quasi-linear behavior; however, the latter area covers a larger extension than its counterpart in the L_1 map. Both the attractors P_1 and P_2 are located on the same side relative to the orbit, thus, the dynamic behavior more closely resembles a single attractor regime. To complete the analysis, the eigenvalue structure of the L_2 Lyapunov family of orbits is also investigated. Figure 11 demonstrates that the system shifts from hyperbolic to nonhyperbolic (or vice versa) along the family, similar to the observations in the L_1 family counterpart. However, these mutations do not seem to affect the attitude behavior as observed on the current map. Nonetheless, extending the integration to two revolutions, new features emerge, as displayed in Fig. 12. Over the longer period, the bottom-right area associated with the quasi-linear motion contracts, but a small double-spike-like region remains for larger A_y amplitudes. The overall double-spike-like region extends approximately from $A_y = 26,800$ to $A_y = 43,800$ km, which locates this zone in the neighborhood of the first bifurcation of the L_2 Lyapunov family (at $Ay \simeq 34,140$ km). At this bifurcation, the system changes from nonhyperbolic to hyperbolic. A similar outcome is also observed in the L_1 Lyapunov family; a double-spike-like region can be located within $A_y = 28,900$ and $A_y = 18,900$ km on the map of Fig. 9, which is in the neighborhood of the first bifurcation of the L_1 Lyapunov family (at $A_y = 21,640$ km). Further analysis is warranted to better understand the attitude response and its relationship to the eigenvalue structure of the orbital dynamics.

D. Axisymmetric Spinning Satellite

Spinning the spacecraft about one of its principal axes is a common practice to inertially stabilize the pointing direction along that same axis. For spacecraft in a Keplerian orbit about a single body, the vehicle often spins about the $\hat{\boldsymbol{b}}_3$ axis. The spin axis $\hat{\boldsymbol{b}}_3$ and the vector normal to the orbit define a plane, if they are not aligned (there exists a nonzero nutation angle). The precession of that plane relative to an inertial or local reference might be investigated for different spin rates. As the spacecraft spins to maintain the $\hat{\boldsymbol{b}}_3$ pointing, the orientation of the $\hat{\boldsymbol{b}}_1$ and $\hat{\boldsymbol{b}}_2$ axes is usually less relevant; for this reason also, such analysis best applies to axisymmetric satellites. In the current investigation, the spacecraft is initially spinning about $\hat{\boldsymbol{b}}_3$, relative to the inertial frame, at the same rate of rotation as the Earth–Moon line (≈13 deg /day), such that $\phi = 0$ deg for all time if there were no external torques. However, the precession of the plane defined by $\hat{\boldsymbol{b}}_3$ and the orbit normal is a significant three-dimensional phenomenon, beyond the scope of the present work. Further analysis would be necessary to clarify the three-dimensional effects and the impact of different initial spin rates about $\hat{\boldsymbol{b}}_3$. Conversely, this paper is

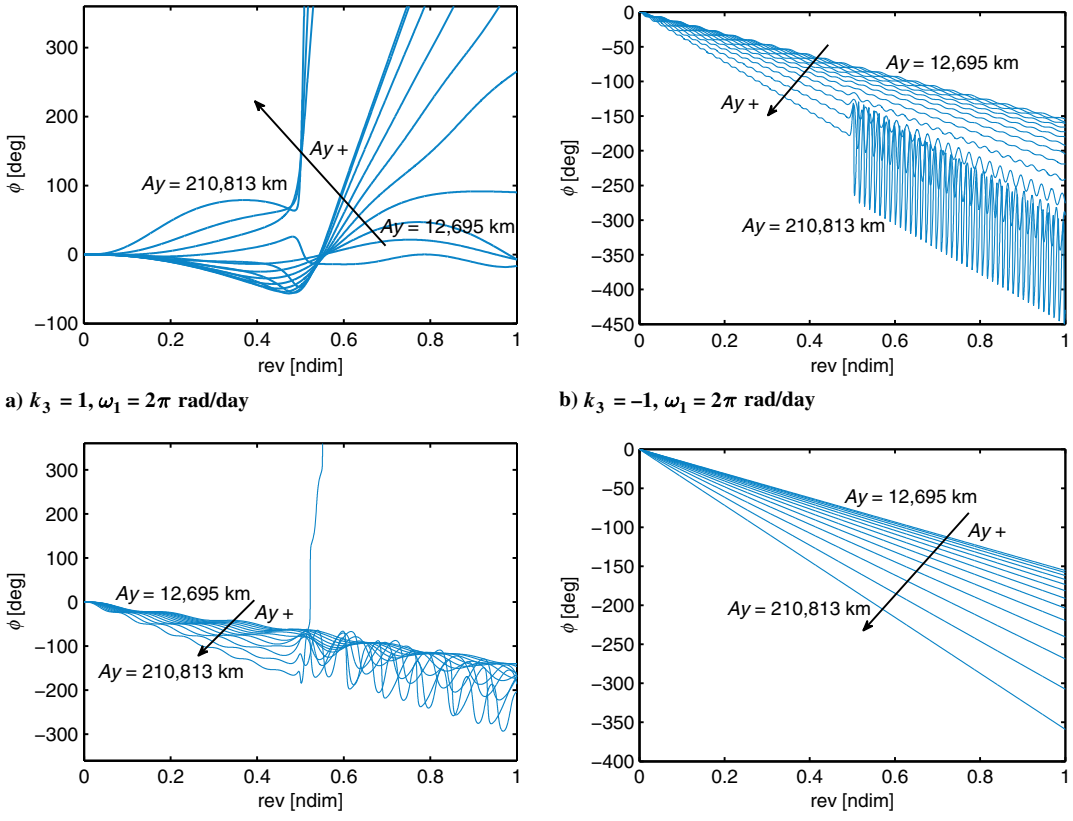

a) $k_3 = 1, \omega_1 = 2\pi$ rad/day

b) $k_3 = -1, \omega_1 = 2\pi$ rad/day

c) $k_3 = 1, \omega_1 = 100\pi$ rad/day

d) $k_3 = -1, \omega_1 = 100\pi$ rad/day

Fig. 13 Effect of the spin about the axis of symmetry $\hat{b}_1$ for different mass distribution.

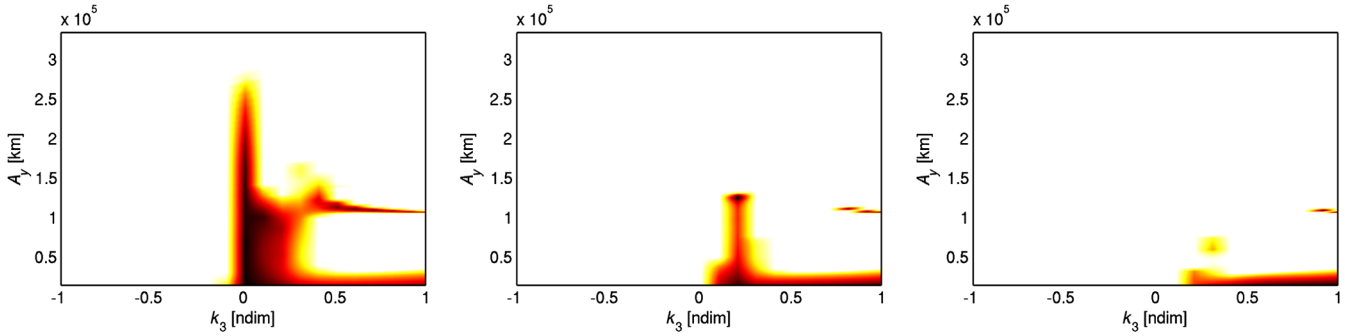

a) $\omega_1 = 0.02\pi$ rad/day b) $\omega_1 = 0.1\pi$ rad/day c) $\omega_1 = 0.2\pi$ rad/day

Fig. 14 Orientation response in ϕ for L_1 Lyapunov family (E-M system) as the spin rate ω_1 varies.

focused on the precession of the $\hat{\boldsymbol{b}}_1$ axis projection in the orbiting plane relative to the Earth–Moon line, which is described by the pitch angle ϕ. Thus, for completeness, any changes in the stability chart of Sec. III.B changes as the vehicle spins about $\hat{\boldsymbol{b}}_1$ is considered. This analysis is conducted on an axisymmetric spacecraft spinning on the axis of symmetry. Let $\hat{\boldsymbol{b}}_1$ be the axis of symmetry and ω_1 the spin rate. In that respect, the inertia ratio $k_3 = 1$ represents a rod-like structure, such that the smallest moment of inertia is about the axis of symmetry; conversely, $k_3 = -1$ denotes a disk-like structure, such that the largest moment of inertia is about the axis of symmetry.

Figure 13 reports some illustrative responses across orbits of the L_1 Lyapunov family as the spin rate ω_1 and the inertia ratio k_3 vary. Each orbit is identified by its A_y amplitude; A_y ranges from 12,695 to 210,813 km. As evident in Fig. 13a for $k_3 = 1$, a small spin rate might not significantly affect the pitch angle dynamics: The response over one revolution stays bounded for a spacecraft orbiting a small amplitude L_1 Lyapunov orbit; conversely, the motion diverges quickly as the amplitude of the orbit increases. During the transition to larger orbits, it is also possible to observe a bounded solution that belongs to the horizontal stable region discussed in Sec. III.B. If the spacecraft is revolving sufficiently fast, the spin axis can be inertially stabilized so that it would be pointing a fixed direction in the inertia I frame. An axis fixed in the inertial frame would appear linearly precessing in the rotating $\mathcal{C}$ frame. This phenomenon can be observed in Fig. 13d, as ϕ describes the orientation of the vehicle relative to the $\mathcal{C}$ frame. The threshold value of ω_1 that inertially fixes $\hat{\boldsymbol{b}}_1$ depends on the mass distribution of the structure; $\omega_1 = 2\pi$ seems to be already effective on a disk-like structure with $k_3 = -1$, as seen in Fig. 13b. Nonetheless, the same spin rate $\omega_1 = 2\pi$ does not alter the dynamics of a rod-like structure with $k_3 = 1$ (see Fig. 13a). However, the transition of the pitch angle motion from solutions essentially not impacted by ω_1 to those that reflect linear precessing motions is not sharp. Further studies are warranted to investigate the intermediate regime. Moreover, the close passage by the Moon at 0.5 revolution is a relevant dynamic event for larger Lyapunov orbits. In fact, not only can it generate the large oscillations of the pointing direction $\hat{\boldsymbol{b}}_1$ depicted in Fig. 13b, but also the close passage can provoke a divergent motion along the larger orbit ($A_y = 210,813$ km) in Fig. 13c.

The Earth–Moon system rotates approximately 13 deg/day relative to an inertial observer. Thus, relative to the Earth–Moon line, an axis that is inertially fixed is likely to precess more than 90 deg over one period of a Lyapunov orbit; in such a case, the ϕ solution should appear as unstable in the mapping presented in Sec. III.B. Also, as supported by Fig. 13, lower values of k_3 should appear as unstable on the map at lower ω_1; to recall, the lower the inertia ratio, the lower the rate to inertially point the spin axis. Consistently, the attitude maps in Fig. 14 demonstrate that the alignment with the Earth–Moon line is lost at lower angular rates ω_1 for lower inertia ratios and the map fades from negative to positive values of k_3. Eventually, if the spacecraft is revolving sufficiently fast, any mass configuration (i.e., any k_3 value) will be becoming unstable and the map will be fading to a uniform white.

IV. Conclusions

The overall goal of this research effort is a better understanding of the attitude dynamics for a rigid spacecraft within the context of the circular restricted three-body problem. The analysis is expanded to fully nonlinear orbits while limiting the orbital motion to the planar Lyapunov families about L_1 and L_2 in the Earth–Moon system. Also, the vehicle is only free to rotate in the orbital plane. The equations governing the spacecraft motion are derived via Kane's method, although a Lagrangian procedure yields a consistent set of equations as well as the same response in a simulation algorithm. A large set of simulations explores the attitude behavior across the families, as well as different vehicle configurations. Results are summarized in terms of attitude maps to identify regions (as a function of spacecraft topology and orbit amplitude) where the body remains close to its initial orientation as observed from the rotating frame. The maps not only display features that are consistent with previous studies, but unexpected solutions also emerge.

Acknowledgments

The following organizations are recognized for providing financial support over the course of these studies: the Natural Science and Engineering Research Council of Canada, Zonta International, and the Canadian Space Agency (CSA). Particular thanks is owed to Alfred Ng from the CSA for his support and guidance. The research program was also funded by the Purdue College of Engineering through the Magoon Award, Teaching Assistantship in School of Aeronautics and Astronautics, and the Future Faculty Fellow (FFF) program in the School of Engineering Education. Eric Holloway is thanked for his continual support in the FFF program. Also, recognition is due to the Alta Scuola Politecnica and the Politecnico di Milano, because they both provided funding opportunities to support parts of this work. Finally, the authors thank the anonymous reviewers for their suggestions.

References

[1] Kane, T. R., and Shippy, D. J., "Attitude Stability of a Spinning Unsymmetrical Satellite in a Circular Orbit (Attitude Stability of a Spinning Unsymmetrical Satellite, with Unequal Moments of Inertia, in a Circular Orbit)," *Journal of Astronautical Sciences*, Vol. 10, 1963, pp. 114–119.

[2] Kane, T. R., and Barba, P. M., "Attitude Stability of a Spinning Satellite in an Elliptic Orbit," *Journal of Applied Mechanics*, Vol. 33, No. 2, 1966, pp. 402–405. doi:10.1115/1.3625056

[3] Kane, T. R., and Marsh, E. L., "Attitude Stability of a Symmetric Satellite at the Equilibrium Points in the Restricted Three-Body Problem," *Celestial Mechanics*, Vol. 4, No. 1, 1971, pp. 78–90. doi:10.1007/BF01230323

[4] Robinson, W. J., "Restricted Problem of Three Bodies with Rigid Dumb-Bell Satellite," *Celestial Mechanics*, Vol. 8, No. 2, 1973, pp. 323–330. doi:10.1007/BF01231434

[5] Robinson, W. J., "Attitude Stability of a Rigid Body Placed at an Equilibrium Point in the Restricted Problem of Three Bodies," *Celestial*

Mechanics, Vol. 10, No. 1, 1974, pp. 17–33.
doi:10.1007/BF01261876

[6] Abad, A., Arribas, M., and Elipe, A., "On the Attitude of a Spacecraft near a Lagrangian Point," *Astronomical Institutes of Czechoslovakia Bulletin*, Vol. 40, No. 5, Sept. 1989, pp. 302–307.

[7] Brucker, E., and Gurfil, P., "Analysis of Gravity-Gradient Perturbed Rotational Dynamics at the Collinear Lagrange Points," *Journal of Astronautical Sciences*, Vol. 55, No. 3, 2007, pp. 271–291.
doi:10.1007/BF03256525

[8] Wong, B., Patil, R., and Misra, A., "Attitude Dynamics of Rigid Bodies in the Vicinity of Lagrangian Points," *Journal of Guidance, Control, and Dynamics*, Vol. 31, No. 1, 2008, pp. 252–256.
doi:10.2514/1.28844

[9] Lara, M., Peláez, J., Bombardelli, C., Lucas, F. R., Sanjurjo-Rivo, M., Curreli, D., Lorenzini, E. C., and Scheeres, D. J., "Dynamic Stabilization of L2 Periodic Orbits Using Attitude-Orbit Coupling Effects," *Journal of Aerospace Engineering*, Vol. 4, No. 1, 2012, pp. 73–82.

[10] Sanjurjo-Rivo, M., Lucas, F. R., Peláez, J., Bombardelli, C., Lorenzini, E. C., Curreli, D., Sheeres, D. J., and Lara, M., "On the Dynamics of a Tethered System near the Collinear Libration Points," *AIAA/AAS Astrodynamics Specialist Conference*, Curran Associated, Red Hook, New York, 2008, pp. 3218–3242.

[11] Knutson, A. J., and Howell, K. C., "Application of Kane's Method to Incorporate Attitude Dynamics into the Circular Restricted Three Body Problem," *Spaceflight Mechanics 2012 (Advances in the Astronautical Sciences)*, Vol. 143, Univelt, AAS Paper 2012-243, San Diego, CA, 2012, pp. 12–243.

[12] Knutson, A. J., and Howell, K. C., "Coupled Orbit and Attitude Dynamics for Spacecraft Comprised of Multiple Bodies in Earth-Moon Halo Orbits," *63rd International Astronautical Congress (IAC)*, Curran Associated, Red Hook, New York, Oct. 2012, pp. 5951–5966.

[13] Knutson, A. J., "Application of Kane's Method to Incorporate Attitude Dynamics into the Circular Restricted Three-Body Problem," Ph.D. Dissertation, Purdue Univ., West Lafayette, IN, Dec. 2012.

[14] Guzzetti, D., "Large Space Structures Dynamics in a Multi-Body Gravitational Environment," M.S. Thesis, Politecnico di Milano, Milan, 2012.

[15] Guzzetti, D., Armellin, R., and Lavagna, M., "Coupling Attitude and Orbital Motion of Extended Bodies in the Restricted Circular 3-Body Problem: A Novel Study on Effects and Possible Exploitations," *63rd International Astronautical Congress (IAC)*, Curran Associated, Red Hook, New York, Oct. 2012, pp. 5715–5729.

[16] Kane, T. R., and Levinson, D. A., "Formulation of Equations of Motion for Complex Spacecraft," *Journal of Guidance and Control*, Vol. 3, No. 2, March–April 1980, pp. 99–112.
doi:10.2514/3.55956

[17] Banerjee, A. K., "Contributions of Multibody Dynamics to Space Flight: A Brief Review," *Journal of Guidance, Control, and Dynamics*, Vol. 26, No. 3, 2003, pp. 385–394.
doi:10.2514/2.5069

[18] Kane, T. R., and Levinson, D. A., *Dynamics: Theory and Applications*, McGraw–Hill, New York, 1985, pp. 15–50, 158–186.

[19] Kane, T. R., Likins, P. W., and Levinson, D. A., *Spacecraft Dynamics*, McGraw–Hill, New York, 1983, pp. 275–279.

[20] Farquhar, R. W., Dunham, D. W., Guo, Y., and McAdams, J. V., "Utilization of Libration Points for Human Exploration in the Sun-Earth-Moon System and Beyond," *Acta Astronautica*, Vol. 55, No. 3, 2004, pp. 687–700.
doi:10.1016/j.actaastro.2004.05.021

[21] Messerschmid, E., and Bertrand, R., *Space Stations: Systems and Utilization*, Springer–Verlag, New York, 1999, pp. 218–219.